



Research paper

Geochemical and tight reservoir characteristics of sedimentary organic-matter-bearing tuff from the Permian Tiaohu Formation in the Santanghu Basin, Northwest China

Jian Ma ^{a,*}, Zhilong Huang ^a, Shijun Liang ^b, Zaizhen Liu ^a, Hao Liang ^b^a State Key Laboratory of Petroleum Resource and Prospecting, China University of Petroleum, Beijing 102249, China^b PetroChina Turpan-Hami Oilfield Company, Xinjiang 839009, China

ARTICLE INFO

Article history:

Received 13 February 2015

Received in revised form

30 January 2016

Accepted 9 March 2016

Available online 10 March 2016

Keywords:

Tight oil

Tuff

Devitrification

Permian

Santanghu Basin

ABSTRACT

Tuff reservoirs have been found in petroliferous basins but have not been sufficiently studied. The discovery of the Permian Tiaohu Formation reservoir in the Santanghu Basin in Northwest China has offered an excellent opportunity to further enhance our knowledge of the tuff's geochemical and reservoir characteristics. The tuff reservoir has the peculiar property of being a sedimentary organic-matter-bearing tuff. In this study, an integrated analysis of the organic geochemistry, elemental and mineral compositions, quartz crystallinity, pore types, and tight reservoir characteristics was conducted based on samples from the 20–30 m-thick tuffs. The extracted tuff samples have total organic carbon (TOC) values of 0.5–1.0 wt.%, total hydrocarbon yield values of 2–6 mg/g, and hydrogen index values of 20–336 mg HC/g TOC. The organic matter consists predominantly of Type III and II₂ kerogens, and the temperature of the maximum yield of pyrolysis varies from 420 to 450 °C, which reflects the oil-generating capacity of the rock. The physical properties of the tuff are characterised by high porosity (varying from 10% to 25%) and low permeability. The air permeability mainly ranges from 0.01 to 0.50 mD. The devitrification of vitreous textures within the tuff primarily dictates the reservoir's characteristics, i.e., the greater the degree of devitrification, the higher the porosity of the reservoir. Vitric tuffs have reservoirs with higher porosity than crystal-vitric tuffs, and the degree of devitrification is generally controlled by the burial depth (temperature) and organic matter (organic acid) content. Vitric tuffs with high porosity and permeability are usually located far from the crater and within the central–lower part of the reservoir. This research may influence geologists to pay more attention to the exploration value of this special type of reservoir in other regions.

© 2016 Elsevier Ltd. All rights reserved.

1. Introduction

As global demand for oil and gas rises and the output from conventional sources decreases, the development potential of unconventional sources of hydrocarbons has gradually become the new focus of attention in many countries. Shale reservoirs have yielded large amounts of gas from horizontal drilling and multi-stage fracturing technology. This same technology has been applied to tight reservoirs with low porosity and permeability, such as the Bakken Formation in Williston Basin in the United States (Fic

and Pedersen, 2013). Tight oil generally refers to accumulations of petroleum in tight sandstones and tight carbonates (Clarkson and Pedemen, 2011; Jia et al., 2012a,b). Following this rapid expansion in shale gas extraction, tight oil has become the most active field of hydrocarbon exploration and development in the world (Kuhn et al., 2012).

A number of considerable differences exist between the tight oil in the Permian Tiaohu Formation in the Santanghu Basin and tight oil that has been discovered in other areas (Liang et al., 2014). (1) This reservoir is tight tuff, not shale, tight sandstone, or tight carbonate. (2) The oil is medium rather than light oil, with a density of 0.89–0.91 g/cm³. (3) The oil is not *in situ* oil, and no close contact exists between the source rock and the reservoir. (4) The tuff reservoir was formed by the upward migration of oil from the source rocks in the Permian Lucaogou Formation through faults in

* Corresponding author. State Key Laboratory of Petroleum Resources and Prospecting, China University of Petroleum (Beijing), 18 Fuxue Road, Changping District, Beijing 102249, China.

E-mail address: 202majian@163.com (J. Ma).

volcanic lava that was several hundred meters thick. However, the tight oils in the Tiaohu Fm. and elsewhere are all from tight reservoirs. They are unconventional reservoirs, where horizontal wells and multistage hydraulic fracturing are necessary for commercial productivity (Zou et al., 2012; Hegazy, 2013; Khan, 2013).

Explosive volcanic eruptions can produce large amounts of fine-grained pyroclastic material, which may be spread laterally over large areas by wind drift (Kolata et al., 1987; Huff et al., 1992; König et al., 2002; Huff, 2008; Qiu et al., 2014). Tuffs are, in turn, formed from the ash that is ejected during volcanic eruptions (Gong et al., 2010). Sedimentation occurs either when tuffaceous material falls directly into a lake, termed 'primary airfall type', or is transported into a lake by water, i.e., 'water carrying resedimented type' (Atri et al., 1999; Haaland et al., 2000; Dunggen et al., 2010; Qiu et al., 2011). The Tiaohu Fm. tuff was mainly formed by volcanic ash that was deposited into a lake without weathering or extensive transportation. The rapid accumulation of volcanic ash, accompanied by the build-up of gases such as H₂S, SO₂, SO₃, and HCl, led to the deaths of aquatic organisms, which contributed organic matter to the Tiaohu Fm. tuff. Periods of volcanic dormancy then allowed aquatic organisms to become re-established, which resulted in renewed enrichment in organic matter (Wang et al., 2011; Li et al., 2014).

Oil and gas have been discovered in some tuff reservoirs, e.g., the Jatibarang oil and gas field in Indonesia (Thomas Kalan and Sitorus, 1994); the Samgori oilfield in the Republic of Georgia (Grynberg et al., 1993); green tuff oil and gas reservoirs in the Akita and Niigata Basins, Japan (Tomaru et al., 2009); the tuff reservoir in Qingxi Sag, China (Li et al., 2004); the tuff reservoir in the Erlian Basin, China (Gao et al., 2006); and the Urho oilfield in the Junggar Basin, China (Gong et al., 2010). These tuff reservoirs, which lack original sedimentary organic matter, contain few primary interparticle pores; secondary dissolution pores and fractures constitute the main pore types, thus differing greatly from the tuff in the Santanghu Basin.

Therefore, the two principal objectives in this study are as follows: (1) to illustrate the particular characteristics of this type of tight reservoir and to provide insight into the geochemical and petrographic characteristics, pore types, and petrophysical properties of sedimentary organic-matter-bearing tuffs; and (2) to discuss the effect of original sedimentary organic matter on micropore formation in tuffs, the main factors that affect the petrophysical properties of tuff reservoirs, and the distribution of the tuffs. These studies can provide useful data for understanding and predicting tight tuff reservoirs in the Santanghu Basin. Furthermore, the results of this investigation could be useful for researchers in other parts of the world where similar situations are found.

2. Geological setting

The Santanghu Basin, which is located in the north-eastern Xinjiang Uygur Autonomous Region of China, is bordered by the Republic of Mongolia to the north, the Turpan-Hami Basin to the south, and the Junggar Basin to the west. Sandwiched between the Tianshan and Altai mountains, this basin is a superimposed basin that developed over an Early Palaeozoic basement. The Santanghu Basin was a rift basin during the Late Palaeozoic and has been a foreland basin since the Mesozoic (Liu et al., 2010). The basin is aligned NW–SE, measures approximately 500 km long and 40–70 km wide, and covers an area of ~2.3 × 10⁴ km². The Santanghu Basin can be divided into three tectonic units: the NE thrust fold belt, central depression, and SW thrust fold belt (Xu et al., 2013). The central depression belt comprises four uplifts and five sags, of which the Malang Sag, covering an area of ~1800 km², is the

most important secondary structural unit. This depression has been relatively well explored and was thus selected as the focus of this study (Fig. 1a).

The Santanghu Basin was an intraplate rift basin during the Permian (Xiao et al., 2004a, 2004b). The basin has experienced a number of tectonic movements, and the regional faults are well developed (Hu et al., 1999; Li et al., 2005). Volcanoes continued to erupt frequently throughout the Late Palaeozoic, and the faults provided channels for volcanic eruptions. The Lucaogou and Tiaohu Formations developed during a period of active volcanism. Volcanism was weak during the deposition of the Lucaogou Fm., during which mudstones, lime mudstones, dolomitic mudstones, and other lacustrine fine-grained sediments developed, forming excellent source rocks (Gao et al., 2010; Ma et al., 2012). However, volcanism was more intense when the first member of the Tiaohu Fm. was deposited (Zhu et al., 2005). A basalt layer that was 200–600 m thick formed in most parts of the basin because of crustal thinning, asthenospheric upwelling, and lithospheric subsidence (Nelson, 1992; Hu et al., 2000; Chen and Jahn, 2004). Subsequently, the volcanism gradually weakened, and a 20–30 m-thick tuff formed at the bottom of the second member of the Tiaohu Fm. The tuff reservoir contains abundant oil, and many wells have achieved commercial oil after performing hydraulic fracturing with horizontal wells (e.g., Well M58H reached a stable oil flow rate of approximately 20 m³/d after performing hydraulic fracturing for over a year). Lacustrine sediments that consisted primarily of tuffaceous mudstones and mudstones were deposited directly over the tuff reservoir. The burial history in Well M56 suggests that the Tiaohu Fm. reached its maximum palaeoburial depth during the Late Cretaceous and was then uplifted (Fig. 2). Therefore, the main diagenesis (e.g., compaction, mineral growth, and mineral transformation) occurred before the Late Cretaceous. An oil–source correlation has revealed that the crude oil in the tuff reservoir is derived from source rocks in the lower Lucaogou Fm. (Ma et al., 2015). Oil migrated vertically through faults and accumulated in the upper tuff reservoir during the Late Cretaceous (Cao and Liu, 2007), so the tight oil in the Tiaohu Formation was not formed in situ (Fig. 1b).

3. Samples and methods

3.1. Sample selection

Samples were obtained from cores from eight existing drilling wells in the Malang Sag to examine the geochemistry and reservoir characteristics. Samples were obtained from horizontal core plugs (2.5 × 5 cm) that were drilled parallel to the bedding plane to test the porosity, permeability, and pore throat radius. The tuff samples were subjected to an oil-wash treatment prior to the testing because they were oil-bearing. Organic geochemistry, thin section, cathodoluminescence, scanning electron microscope (SEM), pore throat radius, and petrophysical property (porosity and permeability) analyses of the tuffs were undertaken at the State Key Laboratory of Petroleum Resource and Prospecting, China University of Petroleum, Beijing. X-ray diffraction (XRD) analysis of the whole-rock minerals, XRD analysis of the quartz crystallinity, and elemental analysis were completed at the Micro Structure Analytical Lab of Peking University.

3.2. Analysis of organic geochemistry

Pyrolysis analysis of 34 core samples was performed with Rock-Eval. The measured parameters included S₁ (free hydrocarbons), S₂ (hydrocarbons cracked from kerogen), S₃ (carbon dioxide released from organic matter), and T_{max} (temperature of the maximum yield

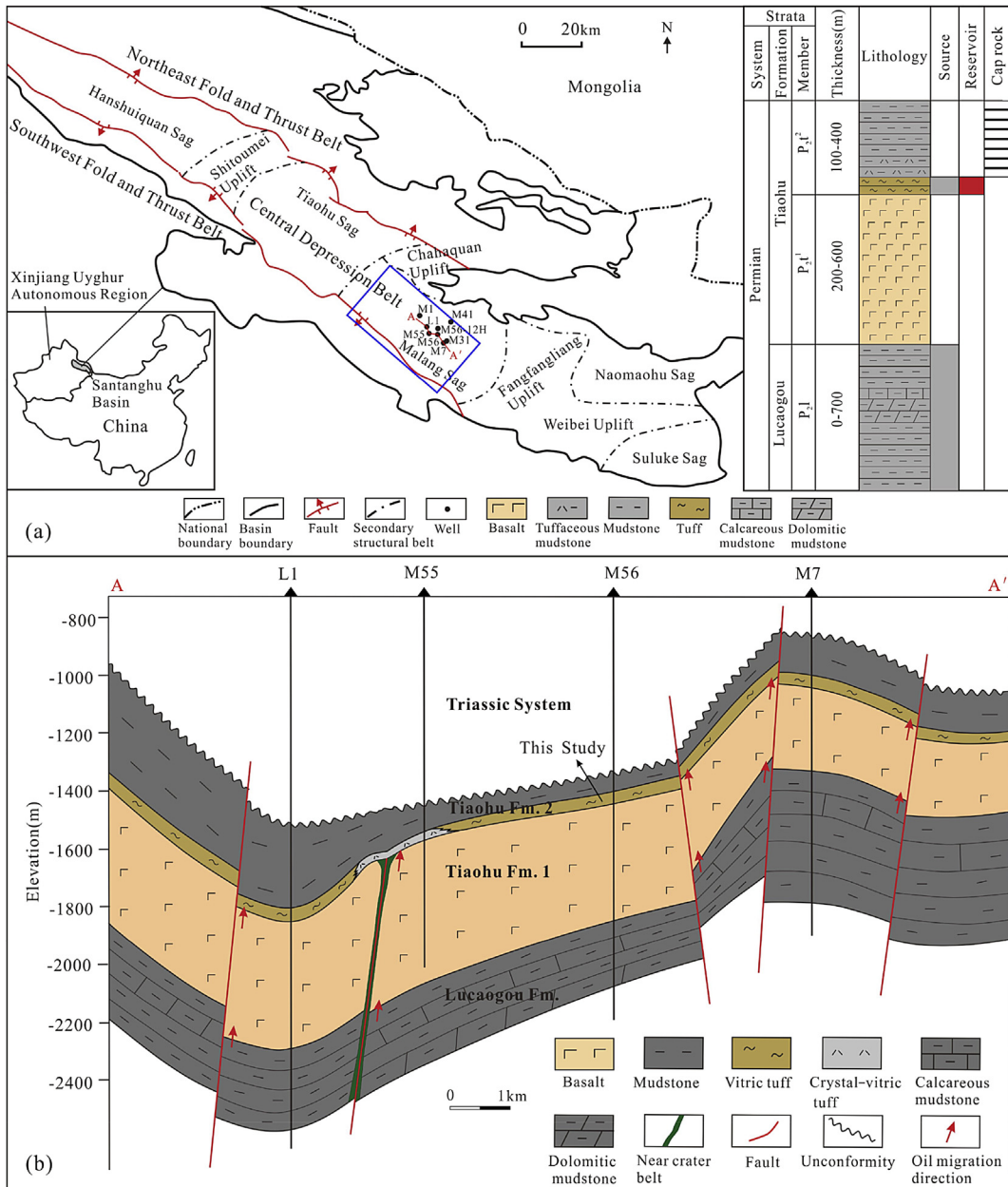


Fig. 1. (a) Location map and regional stratigraphic nomenclature of the Santanghu Basin, NW China. (b) Transverse section across the middle segment of the Malang Sag, exhibiting the source rocks of the Lucaogou Formation at the bottom, tuff reservoir of the Tiaohu Formation at the top, and migration pathways through the fractures.

of pyrolysatate). The total organic carbon (TOC) was determined by using a CS230HC organic carbon analyser. The measurement technique was based on the combustion of the sample in an oxygen environment to convert the TOC to CO₂; then, the hydrogen index (HI) was calculated with S₂ and TOC.

3.3. Analysis of reservoir characteristics

Thin sections of the core samples were observed under polarised and cross-polarised light with a microscope. The CL8200 MK5-2 optical cathodoluminescence system was used at room temperature to identify the mineral composition and size distribution. First, the thin sections were vacuumised; next, cathode rays were emitted, and images were obtained when the vacuum was <0.5 mB. The beam current was set at 270 μA and the beam voltage was set at

15 kV to contrast the emission intensity. Small samples of massive tuff were selected, and their fresh surfaces were coated with gold. Then, the morphologies and pore types of the tuff samples were observed by using a high-resolution field emission scanning electron microscope (FEI Quanta200) combined with secondary electron, Ar-ion-beam milling, and backscattered electron imaging. The tuff core samples were crushed to sizes that were <40 μm by using a mortar, and their mineral compositions were determined by XRD analysis with the following parameters: Cu-Kα radiation, 40 kV voltage, 100 mA current, 3–70° scanning range, 0.01° sampling step width, and 4°/min scanning speed. Minerals were recognised according to the diffractogram, and their relative abundances (weight percentages) were analysed semi-quantitatively. An XRD technique was also employed to determine the quartz crystallinity, and quartz crystallinity indices (QCIs) were determined according to the

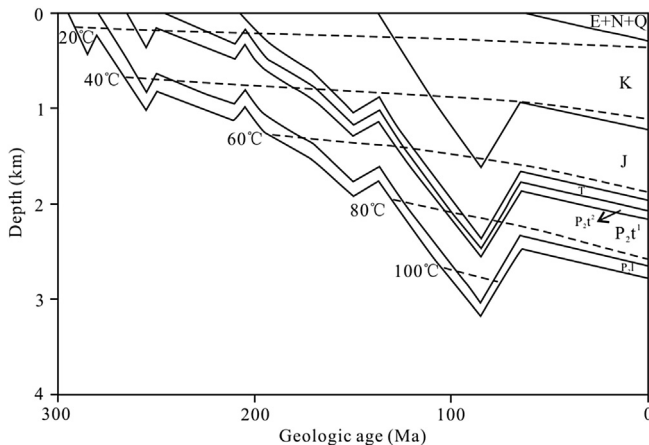


Fig. 2. Burial history in Well M56 in the Santanghu Basin (see Fig. 1 for location). P_2t = Lucaogou Formation; P_2t^1 = first member of Tiaohu Formation; P_2t^2 = second member of Tiaohu Formation; T = Triassic system; J = Jurassic system; K = Cretaceous system; E+N+Q = Cenozoic strata.

method of Murata and Norman (1976). Diffractograms were recorded from 66 to 70° (2θ) by using the step-scan method under analysis conditions of 40 kV and 100 mA with Cu-K α radiation. Five measurements were recorded for each sample, with the powder remounted in the holder for each measurement. The step width and slit sizes were 0.01° /step (0.5° /min), DS (divergent slit) = 1° , RS (receiving slit) = 0.3 mm, and SS (scatter slit) = 1° . The instrumental correction factor F was calculated by using synthetic standard quartz. The QCI was given as $QCI = 10 \times F \times (a/b)$. The QCI of standard quartz is 10 ; thus, the value of F was calculated as 1.48 . The parameter 'a' represents the difference from the peak to the valley (peak (67.7°) – valley (67.8°)) in the diffractograms. The parameter 'b' represents the difference from the peak (67.7°) to the background line. Analyses of the major and trace elements in the tuffs were conducted by using X-ray fluorescence (XRF) and Inductively Coupled Plasma-Atomic Emission Spectrometry (ICP-AES) (PerkinElmer Optima 8300 Series), respectively. The porosity and permeability were tested by using helium and nitrogen, respectively, with the gas-testing method (PDP-200). The pore throat radii of the tuffs were determined by using a high-pressure mercury injection meter (PoreMaster GT60).

4. Results

4.1. Geochemical characteristics of sedimentary organic matter

Direct measurements of the TOC in the tuff samples do not indicate the abundance of sedimentary organic matter because the Tiaohu Fm. tuff is a reservoir filled with oil. Thus, the characteristics of the original sedimentary organic matter cannot be determined until the crude oil or bitumen within the rocks has been completely extracted. Table 1 shows considerable variation in the TOC of the tuff before and after hydrocarbon extraction. Therefore, only the TOC values of the samples after extraction can be used for the evaluation index of the hydrocarbon potential. The TOC of the tuffs in the second member of the Tiaohu Fm. reflects the low abundance (0.5–1.0 wt.%) of sedimentary organic matter (Fig. 3a). The total hydrocarbon yield ($S_1 + S_2$) values are mainly 2–6 mg/g (Fig. 3b), and the HI values are 20–336 mg HC/g TOC (average: 154 mg HC/g TOC). A plot of the HI versus the pyrolysis T_{max} , which is usually used to classify the maturity and type of organic matter (Tissot and Welte, 1984), shows that the organic matter in the tuff samples consist predominantly of Type III and II₂ kerogens, although a few

samples are located in the Type II₁ kerogen area (Fig. 3c). The T_{max} values primarily vary from 420 to 450 °C, which indicates that the maturity of the organic matter is not high. The measured Ro (vitrinite reflectance) of the Lucaogou Fm. source rocks is mainly 0.7–0.9%. Because the tuffs were buried at shallower depths than the Lucaogou Fm.'s source rocks, the maturity of the tuffs' sedimentary organic matter is conjectured to be slightly lower.

4.2. Characteristics of the tuff tight reservoir

4.2.1. Major and trace elements

The crystal fragments in the Tiaohu Fm. tuffs chiefly consist of quartz and albite. Pyroxene, olivine, and other dark minerals are rarely observed. The composition of vitric fragments is largely felsic (mainly Si and O, followed by Al, Na, K, and small amounts of Mg, Fe, and Ca). These characteristics indicate that the erupted magmas possess features of acidic volcanic rocks. Felsic tuffs are common throughout the Late Permian Newcastle and Wollombi Coal Measures in the northern Sydney Basin. The Nb/Y and Zr/TiO₂ ratios show that the tuffs were derived from rhyodacitic to dacitic magmas (Krame et al., 2001). Overall, 19 tuff core samples from the Tiaohu Fm. were selected for major and trace element analyses. The results demonstrate that the SiO₂ content ranges from 52.91 to 73.02% (average: 62.29%). The TAS diagram (Fig. 4a) shows that the tuff samples are largely situated in intermediate-acid volcanic rock (rhyolite, dacite, and trachyandesite) areas. The data points in the Nb/Y–Zr/TiO₂ diagram of the trace elements in the Tiaohu Fm. tuffs are largely located within the intermediate-acid volcanic areas of andesite and rhyodacite–dacite (Fig. 4b), which indicates the primarily intermediate-acid nature of the original volcanic ash.

4.2.2. Petrography

Massive and earthy yellow tuffs with poor stratification occur in the Permian Tiaohu Fm. in the Santanghu Basin (Fig. 5a and b). The original composition of vitric tuff is mainly vitric fragments with a high degree of devitrification. The microcrystals largely exhibit extinction under cross-polarised light (Fig. 5c and d). Crystal-vitric tuff is mainly composed of vitric fragments (content >50%) with some crystal fragments (Fig. 5e and f). The formation temperature of quartz and other minerals can be reflected by the cathodoluminescence technique. For example, under cathodoluminescence, quartz that formed at high (>573 °C), medium–high (300–573 °C), and low (<300 °C) temperatures appears bluish-purple, brownish-red, and non-luminescent, respectively. In contrast, calcite is orange and feldspar emits variable light (Zhang et al., 2003; Wark et al., 2007; Peng et al., 2010). This study found that most quartz grains in the vitric tuffs were non-luminescent under cathodoluminescence (Fig. 5g and h), which indicates that these grains mostly formed at low temperatures, i.e., as products of devitrification during the diagenesis stage. The mineral tuff compositions measured by XRD, show that the quartz content was the highest (40–70%), followed by albite (10–40%) (Table 2). The overall content of clay minerals was low, and that of vitric tuff clay minerals was extremely low (<10%). Crystal-vitric tuff contains a small amount of clay minerals. Overall, the mineral composition of the tuff is relatively simple, i.e., mainly quartz and feldspar. The clay mineral content is low, with only small amounts of calcite and pyrite, and other minerals are rare.

4.2.3. Quartz crystallinity indices

The X-ray diffractogram (Fig. 6) shows that the peak pattern is more diffusive and becomes broader when the QCI is lower. A complete graphic composed of five sharp peaks appears when the QCI is high (Marinoni and Broekmans, 2013), so the diffractogram directly reflects the quartz crystallinity. For example, the

Table 1

Total organic carbon (TOC) data for tuff samples from the Tiaohu Formation before and after extraction.

Well	Depth (m)	Formation	Lithology	TOC (wt.%, before extraction)	TOC (wt.%, after extraction)
M7	1884.44	P ₂ t ²	Tuff	6.08	1.57
M7	1893.36	P ₂ t ²	Tuff	4.21	2.27
L1	2547.06	P ₂ t ²	Tuff	9.66	3.98
L1	2548.6	P ₂ t ²	Tuff	6.08	1.92
L1	2547.59	P ₂ t ²	Tuff	8.66	3.79
M1	1826	P ₂ t ²	Tuff	3.3	1.46
M1	1831.9	P ₂ t ²	Tuff	2.98	0.85
M1	1832.79	P ₂ t ²	Tuff	2.66	0.83
M1	1828.96	P ₂ t ²	Tuff	3.29	0.89
M15	2345.46	P ₂ t ²	Tuff	4.44	0.94
M55	2270.21	P ₂ t ²	Tuff	2.93	0.98
M56	2141.97	P ₂ t ²	Tuff	6.51	0.77
M56	2142.3	P ₂ t ²	Tuff	5.57	0.15
M56	2143.33	P ₂ t ²	Tuff	6.04	0.81
M56	2145.13	P ₂ t ²	Tuff	4.48	0.34

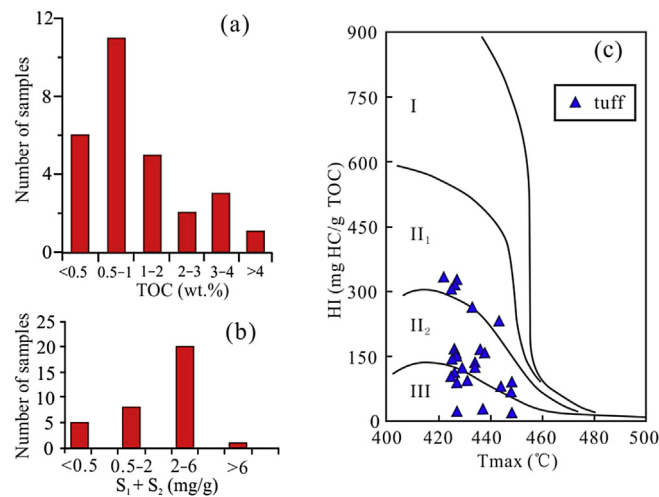


Fig. 3. Geochemical characteristics of tuff samples from the Tiaohu Formation after extraction. (a) Total organic carbon (TOC) distribution, showing the organic matter abundance of the tuffs. (b) Hydrocarbon yield ($S_1 + S_2$) distribution, showing the hydrocarbon-generating potential of organic matter in the tuff. (c) Plot of the hydrogen index (HI) versus the temperature of maximum yield of pyrolylate (T_{max}), showing kerogen types.

at 2266.90 m is relatively diffuse, the background line is curved, and the QCI value is 4.7. The overall quartz crystallinity index of the tuff is high (>5).

According to the correlation between the mineral content and QCI, the quartz content is higher when the QCI value is greater, which signals a positive relationship (Fig. 7). However, the QCI value is generally <8.5, and the quartz content does not always increase linearly with the QCI value (Fig. 7). Experimental data also show a positive correlation between the QCI and tuff palaeoburial depth during the Late Cretaceous, i.e., the higher the temperature or depth, the greater the QCI value (Fig. 8). At the same depth, vitric tuff has a higher QCI value than that of crystal-vitric tuff.

4.2.4. Pore types

Pores are difficult to observe in thin sections of tight sedimentary organic-matter-bearing tuff. However, well-developed micro-pores are found under an SEM. The sizes of the individual pores are small, but their numbers are large. The pore size is mainly on the micron–nanometre scale. For the sake of uniformity, the pore classification of Loucks et al. (2012) for unconventional shale is used here. Zhao et al. (2013) also adopted this standard in their study of pore types in organic-matter-rich calcilutite. Matrix-related pores in tuffs can be divided into three types: (1) inter-

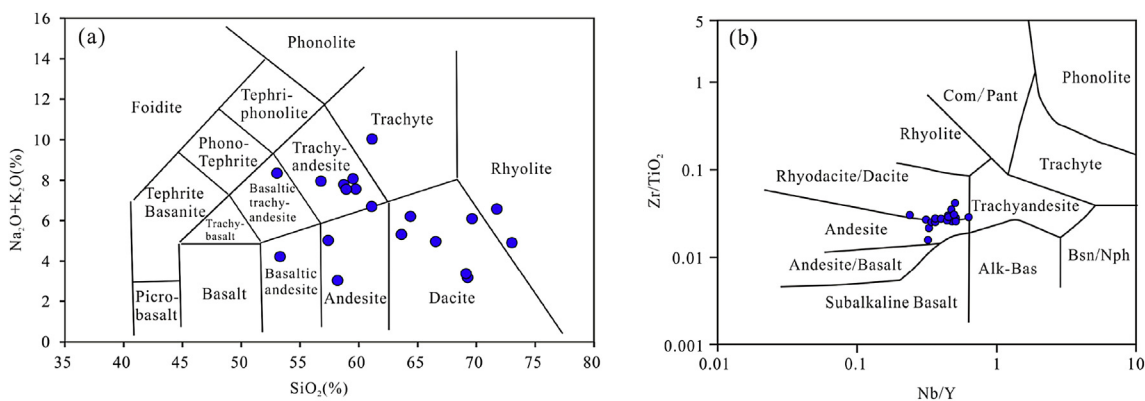


Fig. 4. (a) Classification of the Tiaohu Formation tuffs in TAS (after Le Bas et al., 1986). (b) Nb/Y–Zr/TiO₂ discrimination diagram for the tuffs of the Tiaohu Formation (after Winchester and Floyd, 1977).

diffractogram of the tuff sample from Well M56 at 2144.73 m is clear, the background line is straight, and the measured QCI value is 7.9. Conversely, the diffractogram of the tuff sample from Well M55

particle pores between minerals (mainly quartz and feldspar); (2) intraparticle pores within minerals (mainly feldspar, inorganic minerals, and clay); and (3) pores within organic matter. Fracture-

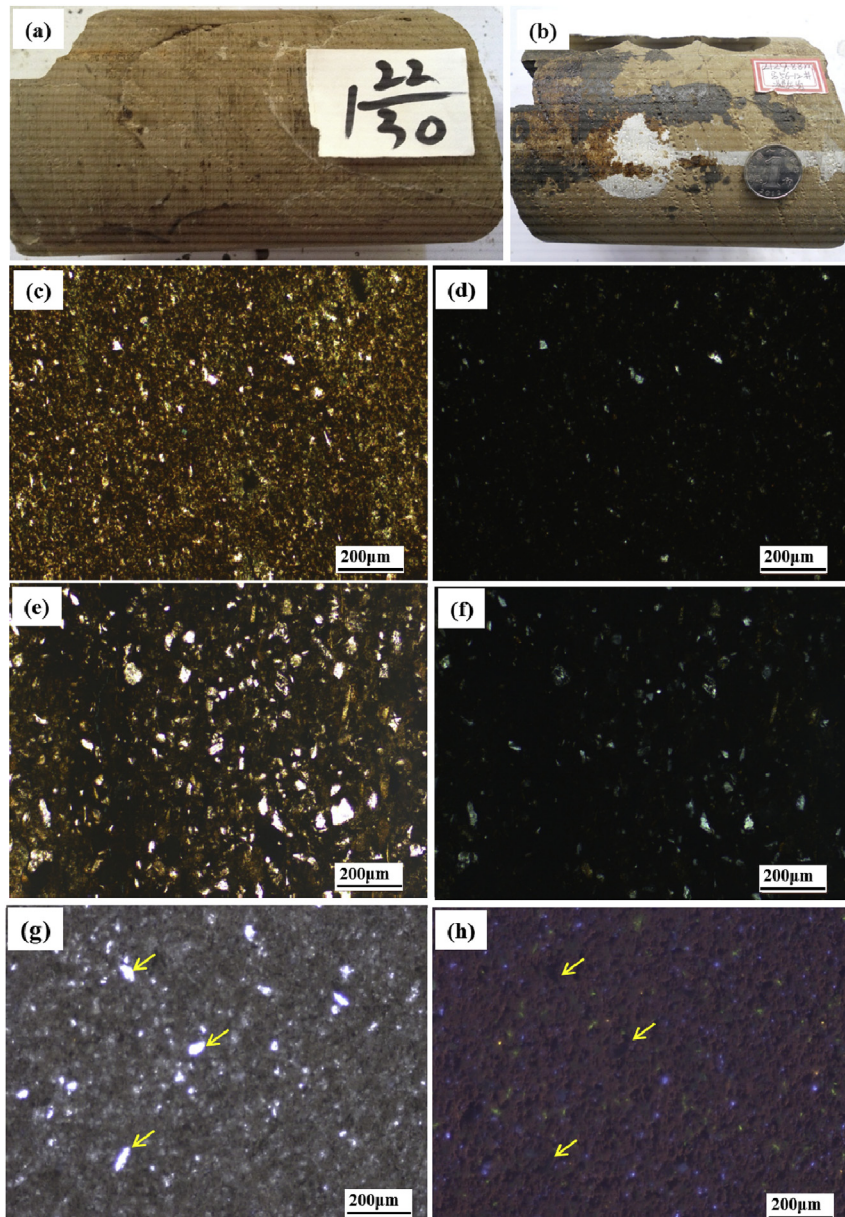


Fig. 5. Petrographic characteristics of the Tiaohu tuffs in the Santanghu Basin. (a) Massive and earthy yellow tuff. Matrix contains oil. Core of Well M56, 2144.72 m, $\Phi = 24.28\%$, $K = 0.165 \text{ mD}$. (b) Massive and earthy yellow tuff. Both matrix and fractures contain oil. Core of Well M56-12H, 2129.88 m, $\Phi = 7.2\%$, $K = 0.0226 \text{ mD}$. (c) Vitric tuff. Core of Well M56, 2142.96 m, $\Phi = 21.6\%$, $K = 0.012 \text{ mD}$, thin section (polarised light). (d) Same source as (c). Obvious extinction is observed. Thin section (cross-polarised light). (e) Crystal-vitric tuff. Core of Well M55, 2267.71 m, $\Phi = 7.1\%$, $K = 0.015 \text{ mD}$. Thin section (polarised light). (f) Same source as (e). Crystal fragments do not show extinction and other parts have obvious extinction. Thin section (cross-polarised light). (g) Vitric tuff. Core of Well M56, 2142.18 m, $\Phi = 14.8\%$, $K = 0.0825 \text{ mD}$. Thin section (polarised light). (h) Same source as (g). Arrows point to non-luminous quartz, showing authigenic quartz formed by devitrification. Thin section (cathodoluminescence). Φ = Porosity; K = Permeability. (For interpretation of the references to colour in this figure legend, the reader is referred to the web version of this article.)

related pores are also present. In this study, most of the interparticle pores between the minerals and intraparticle pores within the minerals formed by devitrification. Thus, these types of pores are collectively referred to as devitrification pores (Zhao et al., 2009).

(1) Interparticle pores

Tuffs are formed from volcanic ash through consolidation and compaction. Volcanic glass is an extremely unstable and mixed component that forms from the rapid cooling of magma and whose composition is mainly silicate, which can be expressed in the form of oxides, e.g., SiO_2 , Al_2O_3 , FeO , Fe_2O_3 , MgO , CaO , Na_2O , K_2O , and

H_2O . Devitrification depends on variations in time, temperature, and pressure during the burial process. Some components are lost with pore water through hydrolysed devitrification. The remaining components are transformed into crystallites or microcrystallites through recrystallisation, and new minerals are formed. The devitrification process comprises vitreous dissolution and precipitation, recrystallisation, migration, the transformation of metal ions, and a series of geochemical processes (McHenry, 2009; Kirov et al., 2011). The formation of new minerals is associated with volume decreases, and a large number of micropores form between different minerals. Interparticle pores between minerals or inter-crystalline pores between microcrystallites are mainly formed by

Table 2

Relative content of different minerals in the Tiaohu Formation tuffs from X-ray diffraction analysis.

Well	Depth (m)	Lithology	Relative content of minerals (%)				
			Quartz	Potassium feldspar	Albite	Clay minerals	Calcite
L1	2547.47	Vitric tuff	45	6	11	5	33
L1	2547.86	Vitric tuff	75	—	16	7	2
L1	2548.78	Vitric tuff	76	6	8	4	6
L1	2548.7–2548.8	Vitric tuff	56	—	20	9	15
L1	2548.9	Vitric tuff	47	—	15	11	27
M56	2141.6–2141.8	Vitric tuff	63	—	33	—	4
M56	2142.2–2142.3	Vitric tuff	57	—	36	—	7
M56	2142.5–2142.6	Vitric tuff	51	—	35	4	10
M56	2142.8–2142.96	Vitric tuff	67	—	29	4	—
M56	2143.6–2143.7	Vitric tuff	43	—	42	9	6
M56	2144.1–2144.4	Vitric tuff	49	—	46	5	—
M56	2144.9–2144.6	Vitric tuff	32	—	58	—	10
M56	2144.73	Vitric tuff	69	—	19	4	8
M56	2145.3–2145.4	Vitric tuff	36	—	57	4	3
M7	1790.8–1790.9	Vitric tuff	66	—	9	14	11
M7	1885.06	Vitric tuff	57	—	37	6	—
M56-12H	2112.7–2112.8	Vitric tuff	78	—	15	7	—
M56-12H	2118.2–2118.3	Vitric tuff	52	—	36	12	—
M56-12H	2118.4–2118.5	Vitric tuff	58	—	23	19	—
M56-12H	2118.9–2119.1	Vitric tuff	68	—	28	4	—
M56-12H	2122.4–2122.6	Vitric tuff	45	—	38	17	—
M56-12H	2125.7–2125.9	Vitric tuff	57	—	36	7	—
M55	2269.15–2269.25	Crystal-vitric tuff	40	—	24	13	23
M55	2270.33–2270.48	Crystal-vitric tuff	45	—	21	28	6

devitrification, which can constitute approximately 70% of the pore types in tuffs (Zhao et al., 2009). Interparticle pores that form by devitrification are mainly pores between quartz and feldspar, which can be clearly observed under an SEM (Fig. 9a and 9b).

(2) Intraparticle pores

Intraparticle pores in the Tiaohu Fm. tuffs comprise dissolution intraparticle pores within feldspar grains, intercrystalline intraparticle pores within a pyrite framboid, and pores within the clay minerals. Dissolution intraparticle pores commonly appear within feldspar grains that were produced by devitrification and in crystal fragments of feldspar in tuffs (Fig. 9c). Energy dispersive spectrometer analysis shows that the major compositions of the minerals within which dissolution intraparticle pores developed mainly include O, Si, Al, and Na. Pyrite also developed in the tuff, which demonstrates that the material formed in a reducing environment. The pyrite framboids include many pyrite crystals, among which micropores act as storage space (Fig. 9d). Although the clay mineral content in the tuff is very low, the main clay mineral is chlorite, in the form of cleavage-sheet shapes with micropores among them (Fig. 9e).

(3) Organic matter pores

Sedimentary organic-matter-bearing tuff reflects a mature evolution stage, with some organic matter pores remaining after hydrocarbon generation. Circular, ovular, or irregularly shaped organic matter pores in tuffs can be recognised by Ar-ion-beam milling. These pores are generally <1.0 μm across, which indicates that most are nanopores. These pores also act as storage space in a tuff tight reservoir that bears organic matter (Fig. 9f). However, not all the organic matter in the study area has developed into pores, and the organic matter pores have very limited impact on the effective pore network.

(4) Fracture-related pores

Fractures have a significant effect on hydrocarbon production. Even when cemented and impermeable, fractures can still influence induced fracture propagation (Gale et al., 2007; Loucks et al., 2012). Many structural fractures, generally including high-angle fractures that are filled with calcite cements, are observed in the tuff cores. A negative relationship exists between the bed thickness of the tuff and the fracture distribution. Core observations show that many open fractures are associated with residual oil, which suggests that these fractures were important hydrocarbon migration pathways (Fig. 10a). Furthermore, open microfractures (mostly <6 μm wide) are also seen under the microscope (Fig. 10b).

4.2.5. Reservoir petrophysical properties and pore throat structure

According to 72 porosity and permeability measurements, the sedimentary organic-matter-bearing tuff in the Tiaohu Fm. is characterised by high porosity and low permeability. The porosity of the tuff ranges from 5% to 25%, and the air permeability is <1.0 mD under atmospheric pressure conditions (Fig. 11). The porosity and permeability of vitric tuff is higher than that of crystal-vitric tuff. Based on 41 measurements, the porosity of the vitric tuff ranges from 13% to 25% (average: 20.6%), and the permeability ranges from 0.001 to 1.0 mD (average: 0.135 mD) (Fig. 11). According to 31 measurements, the porosity of the crystal-vitric tuff ranges from 5% to 18% (average: 11.7%), and the permeability ranges from 0.001 to 0.1 mD (average: 0.029 mD) (Fig. 11).

The pore throat radius of the Tiaohu tuff is small under atmospheric pressure conditions (Fig. 12). Fig. 12a shows that the calculated pore throat radii of the tuff are generally <1.0 μm, which indicates micropores. According to 48 measurements of the average pore throat radius and porosity, the average pore throat radius is generally <0.25 μm; the larger the average pore throat radius, the higher the porosity (Fig. 12b). The average pore throat radius of the vitric tuff ranges from 0.04 to 0.25 μm (average: 0.12 μm). The average pore throat radius of the crystal-vitric tuff ranges from 0.003 to 0.05 μm (average: 0.02 μm).

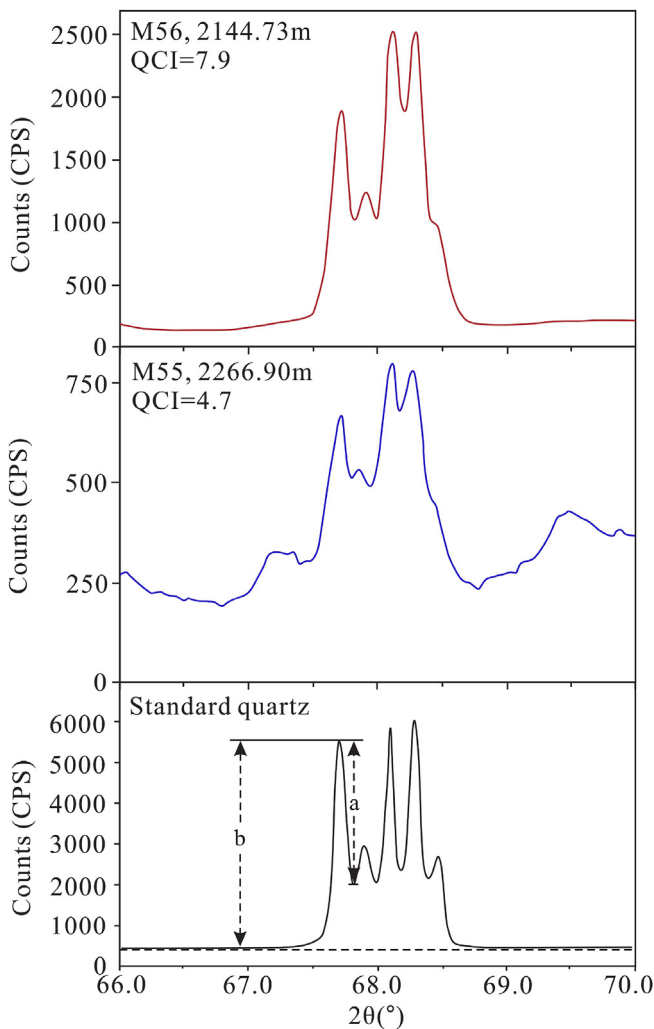


Fig. 6. X-ray diffraction spectra for determination of quartz crystallinity index (QCI). The parameter 'a' represents the difference from the peak to the valley (peak (67.7°) – valley (67.8°)) in the diffractograms. The parameter 'b' represents the difference of the peak (67.7°) to the background line.

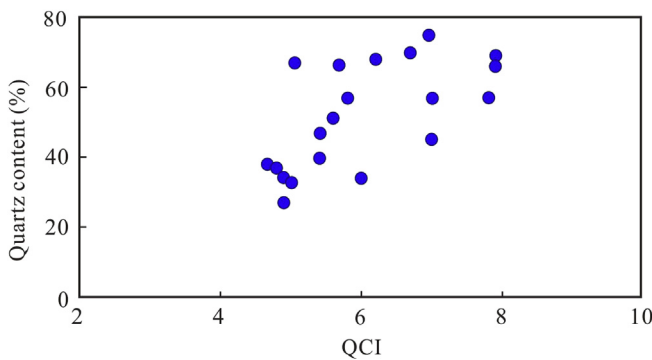


Fig. 7. Plot of quartz crystallinity index (QCI) versus quartz content of the Tiaohu Formation tuffs.

5. Discussion

5.1. Effects of sedimentary organic matter on pore formation

Original sedimentary organic matter is present in the tuff in the

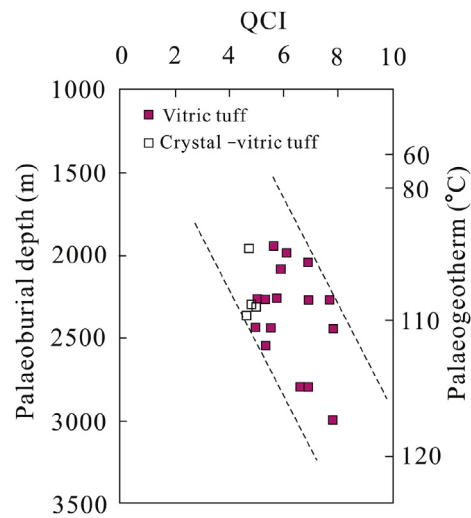


Fig. 8. Plot of palaeoburial depth of the Late Cretaceous (palaeogeotherm) versus quartz crystallinity index (QCI) of the Tiaohu Formation tuffs. QCI is also controlled by the lithology of the tuffs, with overall lower QCI values for crystal-vitric tuffs.

Tiaohu Fm. One reason for the presence of sedimentary organic matter could be that nutrients that are released rapidly into the water by volcanic ash promote biological blooms (Delmelle et al., 2007; Langmann et al., 2010; Lin et al., 2011). Another reason could be that pyrite is observed in the tuff cores, which suggests a reducing environment that was favourable to the preservation of organic matter (Demaison and Moore, 1980; Graciansky et al., 1984). However, the organic matter abundance in the tuff is not high, which may have been caused by rapid volcanic ash deposition from localised eruptions and thus resulted in few clastic interlayers in the 20–30 m-thick tuffs. Rapid deposition has a diluting effect on organic matter (Stein, 1986, 1990). However, the organic acids that are produced by sedimentary organic matter in tuff during kerogen maturation (Meshiri, 1986; Barth and Bjørlykke, 1993) dissolve crystal feldspar fragments and feldspar that formed by devitrification. Evidence of feldspar dissolution is clearly observed under an SEM (Fig. 9c). Dissolution micropores are also an important storage space in tuff reservoirs. The original organic matter abundance and porosity show a positive relationship between the TOC of the tuffs after extraction (reflecting the content of the original sedimentary organic matter) and the porosity (Fig. 13a). This observation hints that the organic matter in the tuff does contribute to pore formation, but a quantitative analysis of this contribution cannot be conducted because the formation of reservoir pores is influenced by many other factors.

5.2. Factors that affect tuff reservoir petrophysical properties

5.2.1. Original tuff composition

Very small quartz and feldspar (<3 μm) particles comprise the main mineral composition of the vitric tuff, and the clay mineral content is low, generally <10%. Crystal-vitric tuff is also characterised by higher contents of quartz and feldspar and lower contents of clay minerals (generally 10%–30%). Based on the data, the porosity and permeability of the vitric tuff is higher than those of the crystal-vitric tuff. These observations are the result of devitrification, which only occurs in the vitreous textures of volcanic material components. Therefore, far fewer interparticle pores formed by devitrification in the crystal-vitric tuff than in the vitric tuff, given the same geological conditions. The tuff reservoir petrophysical properties are related to the devitrification of volcanic

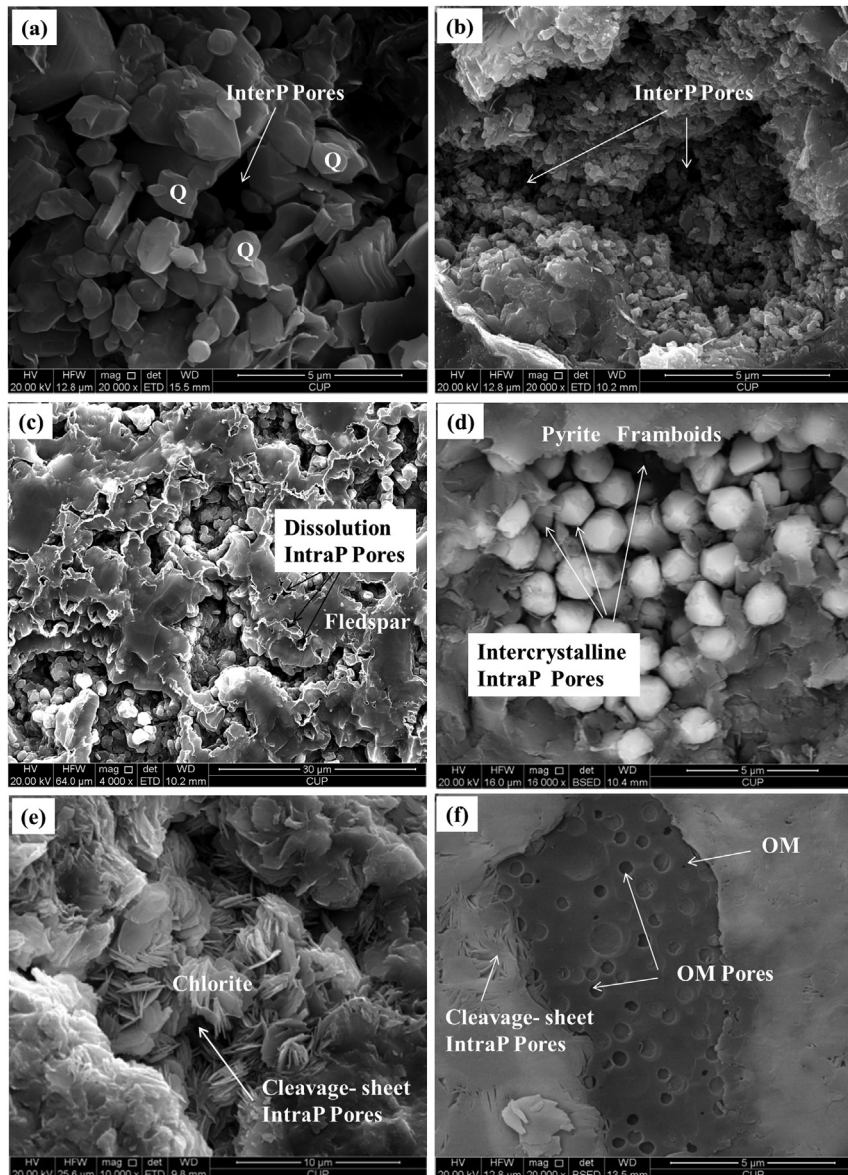


Fig. 9. Examples of different micropores in tuffs of the Tiaohu Formation. (a) Interparticle (InterP) pores between quartz formed by devitrification. Well M56, 2143.3 m, $\Phi = 22.4\%$, $K = 0.134 \text{ mD}$. Observed by FEI-SEM. (b) Interparticle (InterP) pores between quartz and feldspar formed by devitrification. Well L1, 2548.7 m, $\Phi = 24.3\%$, $K = 0.181 \text{ mD}$. Observed by FEI-SEM. (c) Dissolution intraparticle (IntraP) pores within a large feldspar grain. Well M56, 2143.3 m. Observed by FEI-SEM. (d) Intercrystalline intraparticle pores within a pyrite framboid. Well L1, 2548.7 m. BSED image. (e) Cleavage-sheet intraparticle pores within chlorite. Core of Well M56, 2142.5 m, $\Phi = 22.7\%$, $K = 0.08 \text{ mD}$. Observed by FEI-SEM. (f) Micropores within organic matter (OM) observed in ion-milled tuff sample. Cleavage-sheet intraparticle pores within chlorite are also observed. Well L1, 2548.7 m. BSED image. Abbreviations: det = detector; WD = working distance; mag = magnification; HV = high voltage; HFW = horizontal frame width; spot = spot size; BSED = backscattered electron detector. Φ Porosity; K = Permeability.

glass in the tuff. Individual interparticle pores within the tuff, which were produced by devitrification, are small but large in number, resulting in high total porosity. The fine granularity and small pore throat radii of the tuff lead to very low permeability.

5.2.2. Devitrification degree of tuff

Interparticle pores that formed by devitrification constitute the highest proportion because of the very low content of clay minerals and limited contents of organic matter and pyrite in the tuff. These pores constitute the most important pore type in tuff reservoirs, so the factors that affect devitrification similarly influence the physical properties of the reservoir. The devitrification of tuff can be characterised by the crystallinity of quartz, which is the best marker of the degree of devitrification in volcanic glass (Yang, 1993). The QCI

reflects the crystallisation temperature and crystallisation rate when quartz grains are forming, which can vary considerably under different geological conditions (Nagashima et al., 2007; Zhao et al., 2012).

A positive relationship exists between the QCI and the porosity of the tuff, which suggests that a higher degree of devitrification increases the porosity of the reservoir (Fig. 13b). This phenomenon occurs because more quartz minerals are produced with higher degrees of devitrification. Quartz is a rigid mineral whose compressive strength increases with increasingly rigid compositions; therefore, quartz is conducive to the preservation of interparticle pores between mineral grains.

The devitrification of glass is affected by various geological factors, such as the formation temperature, pressure, pH, fluid

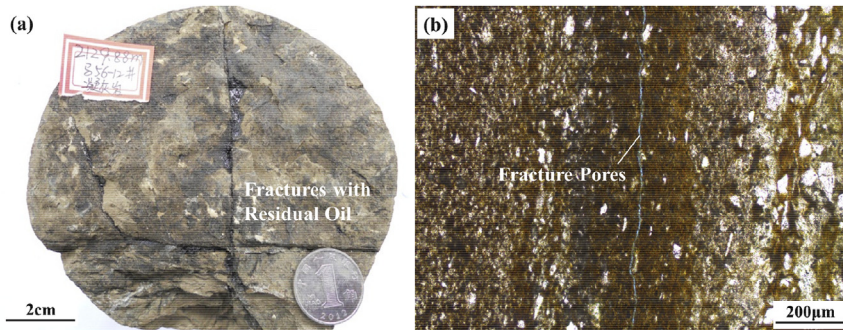


Fig. 10. Examples of fracture pores in tuffs of the Tiaohu Formation. (a) Fractures with residual oil. Core sample of Well M56-12H, 2129.88 m. (b) Opening-mode microfracture. Well M56, 2142.9 m.

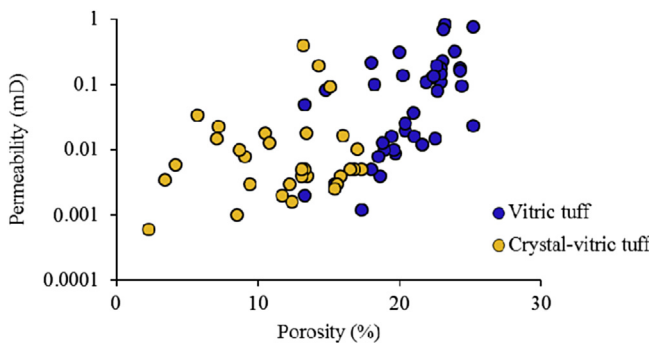


Fig. 11. Plot of porosity versus permeability of the tuffs in the Tiaohu Formation, showing the differences in petrophysical properties between vitric tuffs and crystal-vitric tuffs.

Tiaohu Fm. tuff is related to its sedimentary organic matter content, which consists mainly of Type III and II₂ kerogens. Type III kerogens easily generate organic acids during evolution (Crossey et al., 1986; Chen et al., 1995).

The effect of temperature on the devitrification of organic-matter-bearing tuff is reflected in two aspects: the increase in the degree of thermal evolution and generation of organic acids, and the increase in the devitrification rate as the temperature increases. Considerable amounts of organic acids can be generated by source rocks under a diagenetic temperature of approximately 60 °C (MacGowan and Surdam, 1988). The maximum amount of short-chain carboxylic acids occurs in the range of 75–90 °C, i.e., the peak of oxygen-containing groups that are released by kerogens. As organic matter matures, organic acids are released. The optimal temperature range for the preservation of organic acids is

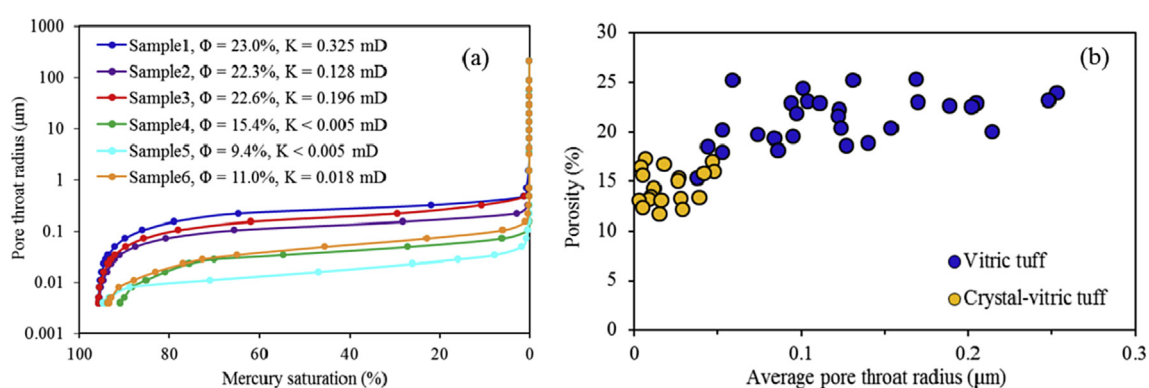


Fig. 12. (a) Pore-throat-size distribution of the Tiaohu Formation tuffs showing nanopores. All six samples are from Well M56-12H (see Fig. 1 for location). K = Permeability; Φ = Porosity. (b) Plot of the average pore throat radius versus porosity of the tuffs in the Tiaohu Formation, which shows the differences in pore throat structures between vitric tuffs and crystal-vitric tuffs.

composition, and velocity. Studies by Gíslason and Oelkers (2003), Wolff et al. (2004), Declercq et al. (2013), and Aradóttir et al. (2013) have shown that the dissolution rates of glassy basalt (basic) and glassy rhyolite (acidic) decrease dramatically with increasing pH under acidic conditions given a single variable of pH, minimise at near-neutral pH, and increase more slowly with increasing pH under basic conditions. All other factors being equal, the higher the temperature, the faster the dissolution rate (Fig. 14). Acidic conditions favour the dissolution of natural Al-silicate volcanic glasses, the removal of metals from the glass structure via proton exchange reactions, and the precipitation of silica (and therefore devitrification) (Declercq et al., 2013). The high degree of devitrification in the

80–120 °C. When the temperature rises to 120–160 °C, carboxylate anions are converted to hydrocarbons and CO₂ through thermal decarboxylation and dicarboxylic acid is converted to monocarboxylic acid. The concentration of CO₂ in the solution increases significantly, but the concentration of organic acids decreases (Sun et al., 2004; Xi et al., 2012). Because the Tiaohu Fm. organic-matter-bearing tuff in the Malang Sag was buried the deepest and reached the highest geotherm (90–100 °C) during the Late Cretaceous, tuff devitrification is speculated to have mainly occurred before the Late Cretaceous. Experimental data shows a positive correlation between the QCI and the tuff palaeoburial depth during the Late Cretaceous (Fig. 16). The higher the temperature, the greater the

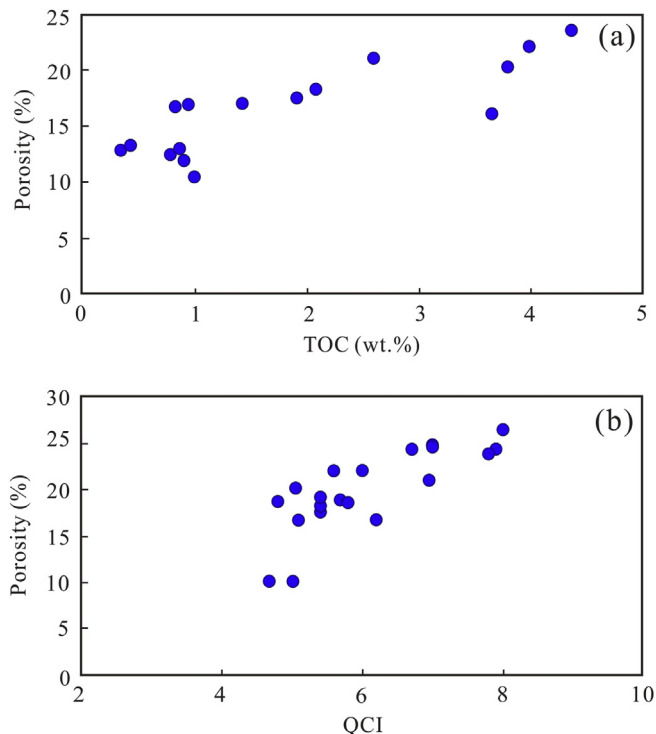


Fig. 13. (a) Plot of total organic carbon (TOC) after extraction versus porosity of the Tiaohu Formation tuffs, showing effect of organic matter on pore formation. (b) Plot of quartz crystallinity index (QCI) versus porosity of the Tiaohu Formation tuffs, showing influence of devitrification degree on reservoir petrophysical properties.

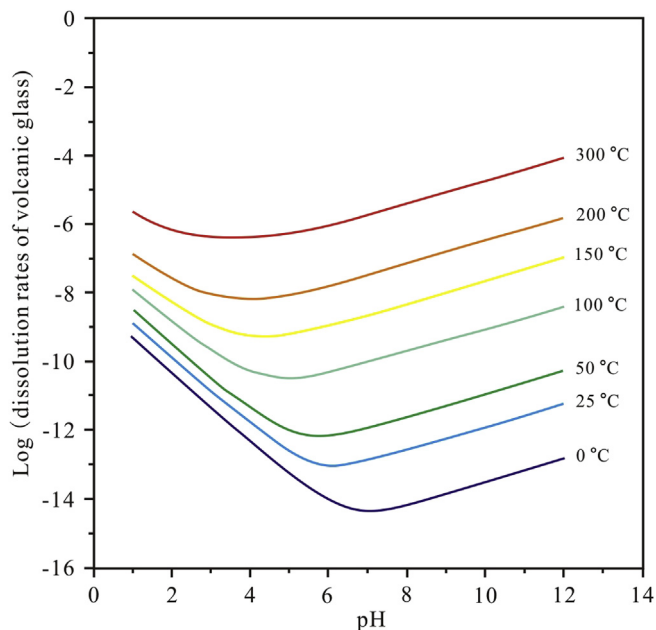


Fig. 14. Dissolution rates of volcanic glass at temperatures from 0 to 300 °C and pH from 1 to 12 (modified after Gíslason and Oelkers, 2003; Aradóttir et al., 2013).

degree of tuff devitrification, although the degree of devitrification is also controlled by the type of tuff.

The physical properties of the reservoir in the organic-matter-bearing tuff from the Tiaohu Fm. are mainly influenced by the original composition of the tuff and the degree of devitrification,

while the organic acid content and burial depth (temperature) are the two most important factors that affect the degree of devitrification.

5.3. Factors that control tuff distribution

The intermediate-acidic tuff of the Tiaohu Fm., which formed at the end of a cycle of volcanic eruptions, is distributed on a set of stable mafic–intermediate volcanic rocks (mainly basalt). These tuffs are the product of the evolution from basic magma to acid magma, and from strong volcanic activity to weak volcanic activity (Howells et al., 1986; Wang et al., 2006). The types of tuff vary with the distance from the crater because of the original material from the volcanic eruption. Sometimes, the tuff distribution can be predicted from the crater distribution (Tan et al., 2012). Generally, the pyroclast content within the tuff increases towards the crater because of the effect of volcanic shard gravity. Within a certain range, the vitric composition of the tuff increases with distance from the crater (Thompson and Hermes, 1990). However, tuffaceous mudstones are found at greater distances from the crater because of the insufficient supply of volcanic ash and increasing shale content (Jiao et al., 2014; Liang et al., 2014). Therefore, the tuff distribution is controlled by the crater. Vitric tuff is usually distributed farther from the crater, crystal-vitric tuff is usually distributed near the crater, and tuffaceous mudstone/siltstone is generally distributed far from the crater (Fig. 15). Vertically, vitric tuff and crystal-vitric tuff are interbedded because of several volcanic eruptions and are usually distributed within the central–lower part of the tuff (Fig. 16). Tuffaceous mudstone is generally vertically distributed within the upper part of the tuff. Occasionally, another special, thin, silicified tuff is present. The silicified tuff is generally distributed within the bottom of the tuff, where it has direct contact with the lower basalt. This tuff is primarily characterised by silicification, with continuous amorphous SiO₂. This type of tuff is very tight, so its resistivity on the well-logging curve is extremely high, usually >300 Ω m.

The distribution of the tuff is also controlled by sedimentary palaeotopography. After entering a lake, the original volcanic ash is deposited by gravity. The palaeotopography of the lake also affects the tuff thickness. Depositional depressions on both sides of the crater are favourable locations for the development of tuffs. Therefore, vitric tuffs with high porosity and permeability are usually located at certain distances from the crater and at moderate depths.

6. Conclusions

The tuff from the Permian Tiaohu Fm. in the Santanghu Basin contains sedimentary organic matter. Extracted tuff samples have TOC values of 0.5–1.0 wt.%, and the organic matter mainly comprises Type III and II₂ kerogens. Organic acids that were produced during kerogen maturation facilitated the process of devitrification and the formation of reservoir micropores.

The petrophysical properties of the tuff reservoir are primarily controlled by the original composition and the degree of devitrification. The porosity and permeability of the vitric tuff is higher than those of the crystal-vitric tuff because of the higher content of vitreous textures, which favours devitrification. The burial depth (temperature) and the content of organic acid are the main factors that control the degree of tuff devitrification in the Santanghu Basin.

The distribution of the tuff is controlled by crater and sedimentary palaeotopography. Vitric tuff with high porosity and permeability is distributed in depressions that are far from the crater, and vertically within the central–lower part of the tuff

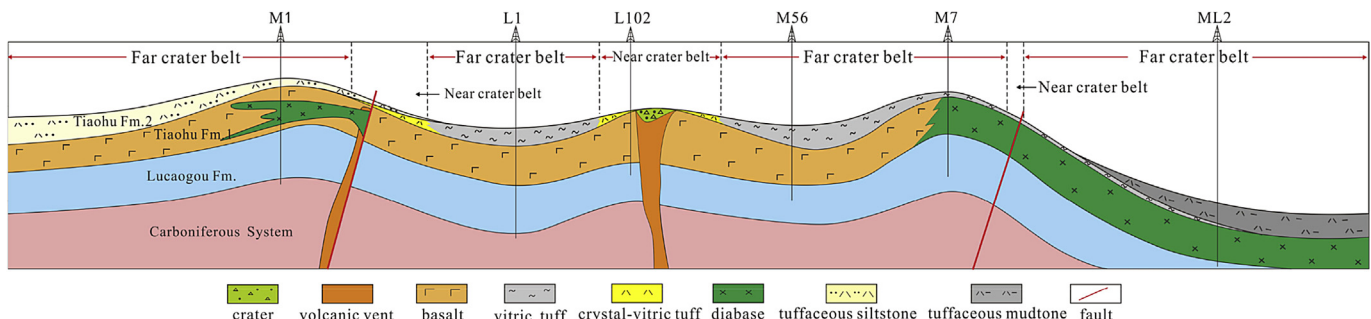


Fig. 15. Distribution pattern of the Tiaohu Formation tuffs in the Malang Sag, showing that the tuffs are controlled by crater and sedimentary palaeotopography. Vitric tuff is distributed in depressions farther from the crater, crystal-vitric tuff is distributed near the crater, and tuffaceous mudstone is distributed far from the crater.

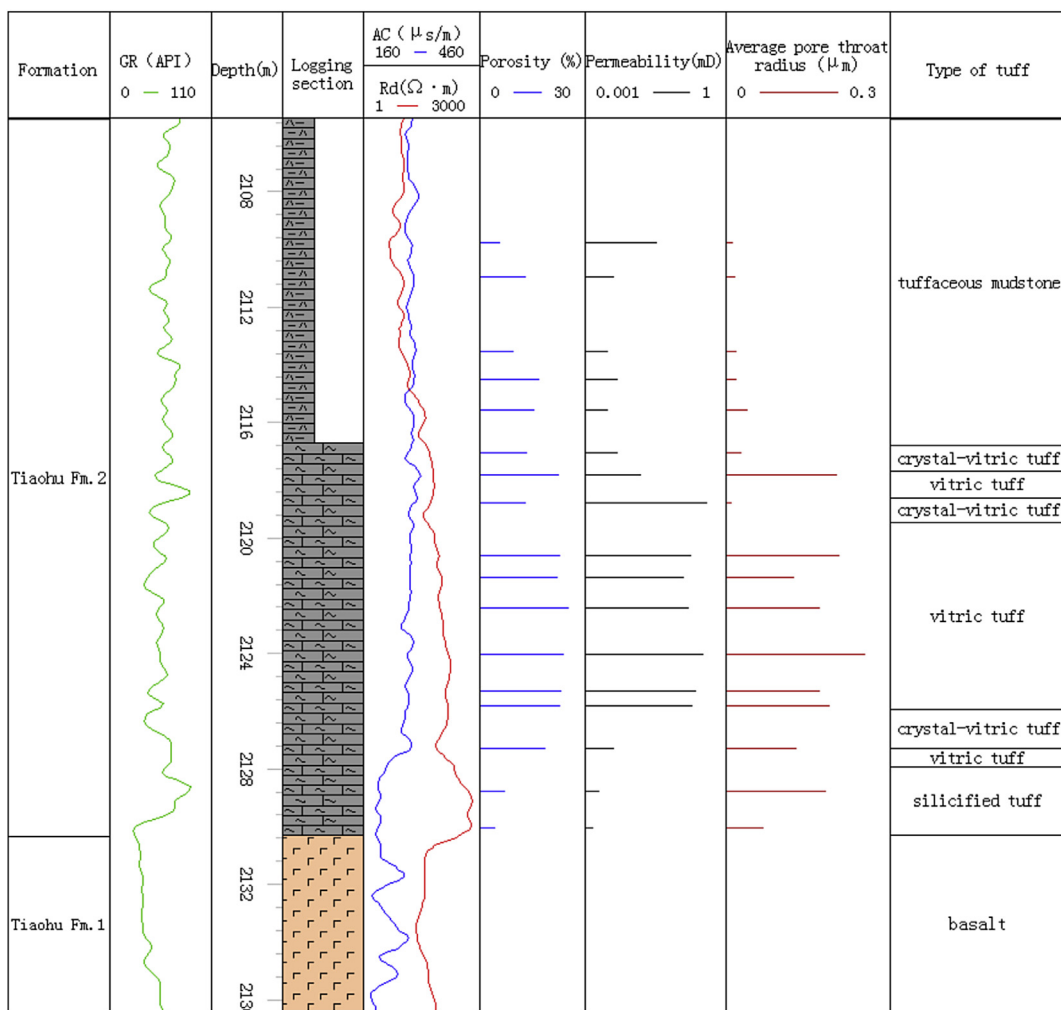


Fig. 16. Vertical distribution characteristics of different types of tuffs (example from Well M56-12H).

reservoir. The discovery of tuff reservoirs in the Santanghu Basin indicates that tuff of a certain thickness is an important type of tight reservoir. However, the relationship between the evolution of organic matter and tuff diagenesis still requires further investigation.

Science Foundation of China (No.: 41472111). The authors thank the PetroChina Turpan-Hami Oilfield Company for providing valuable geological data, as well as crude oil and core samples. We also sincerely thank several anonymous reviewers for their detailed and constructive suggestions, which significantly improved this manuscript.

Acknowledgements

This research was financially supported by the National Natural

References

- Aradóttir, E.S.P., Sigfusson, B., Sonnenthal, E.L., Björnsson, G., Jónsson, H., 2013. Dynamics of basaltic glass dissolution—capturing microscopic effects in continuum scale models. *Geochim. Cosmochim. Acta* 121, 311–327.
- Atri, A.D., Pierre, F.D., Lanza, R., Ruffini, R., 1999. Distinguishing primary and re-sedimented vitric volcanoclastic layers in the Burdigalian carbonate shelf deposits in Monferrato (NW Italy). *Sediment. Geol.* 129, 143–163.
- Barth, T., Bjørlykke, K., 1993. Organic acids from source rock maturation: generation potentials, transport mechanisms and relevance for mineral diagenesis. *Appl. Geochem.* 8, 325–337.
- Cao, Q., Liu, Y.Q., 2007. Application of fluid inclusion to study of petroleum migration in Santanghu Basin, China. *Acta Petrol. Sin.* 23, 2309–2314.
- Chen, B., Jahn, B.M., 2004. Genesis of post-collisional granitoids and basement nature of the Junggar Terrane, NW China: Nd–Sr isotopic and trace element evidence. *J. Asian Earth Sci.* 23, 691–703.
- Chen, C.P., Mei, B., Yi, S.J., Ma, T., Cai, C.F., 1995. An analysis for low molecular weight organic acids in formation waters. *Acta Pet. Sin.* 16, 48–54.
- Clarkson, C.R., Pedemen, P.K., 2011. Production Analysis of Western Canadian Unconventional Light Oil Plays. SPE 149005.
- Crossey, L.J., Surdam, R.C., Lahann, R., 1986. Application of organic/inorganic diagenesis to porosity prediction. *SEPM Spec. Publ.* 38, 147–155.
- Declercq, J., Diedrich, T., Perrot, M., Gislasoñ, S.R., Oelkers, E.H., 2013. Experimental determination of rhyolitic glass dissolution rates at 40–200 °C and 2 < pH < 10.1. *Geochim. Cosmochim. Acta* 100, 251–263.
- Delmelle, P., Lambert, M., Dufrene, Y., 2007. Gas/aerosol-ash interaction in volcanic plumes: new insights from surface analyses of fine ash particles. *Earth Planet. Sci. Lett.* 259, 159–170.
- Demaison, G.J., Moore, G.T., 1980. Anoxic environments and oil source bed genesis. *Org. Geochem.* 2, 9–31.
- Dungan, S., Olgun, N., Croot, P., 2010. The role of airborne volcanic ash for the surface ocean biogeochemical iron-cycle: a review. *Biogeosciences* 7, 827–844.
- Fic, J., Pedersen, P.K., 2013. Reservoir characterization of a 'tight' oil reservoir, the middle Jurassic upper Shaunavon member in the Whitemud and Eastbrook pools, SW Saskatchewan. *Mar. Pet. Geol.* 44, 41–59.
- Gale, J.F., Reed, R.M., Holder, J., 2007. Natural fractures in the Barnett Shale and their importance for hydraulic fracture treatments. *AAPG Bull.* 91, 603–622.
- Gao, G., Li, H.M., Liang, H., 2010. Origin of Jurassic hydrocarbon and accumulation model in Santanghu Basin. *Nat. Gas. Geosci.* 21, 15–18 (in Chinese with English abstract).
- Gao, R.Q., Yang, J.B., Cong, P.D., 2006. Analysis of the characteristics of tuffite reservoir in Erlan oilfield. *Welllogging Technol.* 30, 330–333 (in Chinese with English abstract).
- Gislasoñ, S.R., Oelkers, E.H., 2003. Mechanism, rates and consequences of basaltic glass dissolution: an experimental study of the dissolution rates of basaltic glass as a function of pH and temperature. *Geochim. Cosmochim. Acta* 67, 3817–3832.
- Graciansky, P.C.De., Deroo, G., Herbin, J.P., Magniez, L., 1984. Ocean-wide stagnation episode in the late Cretaceous. *Nature* 22, 346–349.
- Grynberg, M.E., Papava, D., Shengelia, M., Takaishvili, A., Nanadze, A., Patton, D.K., 1993. Petrophysical characteristics of the middle Eocene laumontite tuff reservoir, Samgori Field, Republic of Georgia. *J. Pet. Geol.* 16, 313–322.
- Gong, Q.S., Ni, G.H., Lu, S.P., 2010. Genesis and reservoir features of tuffaceous rocks in Wuerhe oilfield of the Junggar Basin. *Oil Gas Geol.* 31, 481–485 (in Chinese with English abstract).
- Haaland, H.J., Furnes, H., Martinsen, O.J., 2000. Paleogene tuffaceous intervals, Grane Field (Block 25/11), Norwegian North Sea: their depositional, petrographical, geochemical character and regional implications. *Mar. Pet. Geol.* 17, 101–118.
- Hegazy, G.M., 2013. A new strategy to explore tight oil/gas reservoirs—fit for purpose acid fracturing. In: AAPG/EAGE Workshop on Tight Reservoirs in the Middle East.
- Howells, M.F., Reedman, A.J., Campbell, S.D.G., 1986. The submarine eruption and emplacement of the lower rhyolitic tuff formation (Ordovician), N Wales. *J. Geol. Soc.* 143, 411–423.
- Hu, A.Q., Jahn, B.M., Zhang, G.X., 2000. Crustal evolution and phanerozoic crustal growth in northern Xinjiang: Nd–Sr isotopic evidence. Part I. Isotopic characterization of basement rocks. *Tectonophysics* 328, 15–51.
- Hu, B., Guan, Q., Zhu, B.S., Zhang, H.D., 1999. Structure and deformation characteristics in Santanghu Basin. *Xinjiang Pet. Geol.* 20, 374–378 (in Chinese with English abstract).
- Huff, W.D., 2008. Ordovician K-bentonites: issues in interpreting and correlating ancient tephras. *Quat. Int.* 178, 276–287.
- Huff, W.D., Bergström, S.M., Kolata, D.R., 1992. Gigantic Ordovician volcanic ash fall in North America and Europe: biological, tectonomagmatic, and event stratigraphic significance. *Geology* 20, 875–878.
- Jia, C.Z., Zheng, M., Zhang, Y., 2012a. Unconventional hydrocarbon resources in China and the prospect of exploration and development. *Pet. Explor. Dev.* 39, 139–146.
- Jia, C.Z., Zou, C.N., Li, J.Z., Li, D.H., Zheng, M., 2012b. Assessment criteria, main types, basic features and resource prospects of the tight oil in China. *Acta Pet. Sin.* 33, 343–350.
- Jiao, L.X., Liu, J.T., Zhang, H., Feng, Y.Q., Wu, C., 2014. Tight reservoir characteristics and formation conditions of tuff in Santanghu Basin. *Nat. Gas. Sci.* 25, 1697–1705.
- Khan, A.M., 2013. Multi-frac Treatments in Tight Oil and Shale Gas Reservoirs: Effect of Hydraulic Fracture Geometry on Production and Rate Transient. Master of Science in Engineering. The University of Texas at Austin, USA.
- Kirov, G., Samajova, E., Nedialkov, R., 2011. Alteration processes and products of acid pyroclastic rocks in Bulgaria and Slovakia. *Clay Miner.* 46, 279–294.
- Kolata, D.R., Frost, J.K., Huff, W.D., 1987. Chemical correlation of K-bentonite beds in the Middle Ordovician Decorah subgroup, upper Mississippi valley. *Geology* 15, 208–211.
- Königer, S., Lorenz, V., Stollhofen, H., Armstrong, R.A., 2002. Origin, age and stratigraphic significance of distal fallout ash tuffs from the Carboniferous–Permian continental Saar-Nahe basin (SW Germany). *Int. J. Earth Sci.* 91, 341–356.
- Krame, W., Weatherall, G., Offler, R., 2001. Origin and correlation of tuffs in the Permian Newcastle and Wollombi coal measures, NSW, Australia, using chemical fingerprinting. *Int. J. Coal Geol.* 47, 115–135.
- Kuhn, P.P., di Primio, R., Hill, R., Lawrence, J.R., Horsfield, B., 2012. Three-dimensional modeling study of the low-permeability petroleum system of the Bakken Formation. *AAPG Bull.* 96, 1867–1897.
- Langmann, B., Zaksek, K., Hort, M., 2010. Volcanic ash as fertiliser for the surface ocean. *Atmos. Chem. Phys.* 10, 3891–3899.
- Le Bas, M.J., Le Maitre, R.W., Streckeisen, A., Zanettin, B., 1986. A chemical classification of volcanic rocks based on the total alkali-silica diagram. *J. Petrol.* 27, 745–750.
- Li, D.H., Li, J.Z., Huang, J.L., Wang, S.Y., Wang, S.F., 2014. An important role of volcanic ash in the formation of shale plays and its inspiration. *Nat. Gas. Ind.* 34, 56–65 (in Chinese with English abstract).
- Li, J., Wang, W., Wang, S.X., 2004. Bedded tuff reservoir in Qingxi oilfield. *Xinjiang Pet. Geol.* 25, 288–290 (in Chinese with English abstract).
- Li, W., Zhou, D.W., Liu, Y.Q., Liang, J.W., 2005. The division of Permian tectonic sequence and the feature of residual tectonic in Santanghu Basin. *J. Northwest Univ. Nat. Sci. Ed.* 35, 617–620 (in Chinese with English abstract).
- Liang, H., Li, X.N., Ma, Q., Xiang, H., Luo, Q.S., Chen, X., 2014. Geological features and exploration potential of Permian Tiaohu Formation tight oil, Santanghu Basin, NW China. *Pet. Explor. Dev.* 41, 563–572.
- Lin, I.I., Hu, C.M., Li, Y.H., 2011. Fertilization potential of volcanic dust in the low-nutrient low-chlorophyll western North Pacific subtropical gyre: satellite evidence and laboratory study. *Glob. Biogeochem. Cycles* 25, 1–12.
- Liu, Y.Q., Li, H., Zhu, Y.S., 2010. Permian lacustrine eruptive hydrothermal dolomites, Santanghu basin, Xinjiang province. *Acta Sedimentol. Sin.* 28, 861–865 (in Chinese with English abstract).
- Loucks, R.G., Reed, R.M., Ruppel, S.C., Hammes, U., 2012. Spectrum of pore types and networks in mudrocks and a descriptive classification for matrix-related mudrock pores. *AAPG Bull.* 96, 1071–1098.
- Ma, J., Huang, Z.L., Gao, X.Y., Chen, C.C., 2015. Oil–source rock correlation for tight oil in tuffaceous reservoirs in the Permian Tiaohu Formation, Santanghu Basin, northwest China. *Can. J. Earth Sci.* 52, 1014–1026.
- Ma, J., Huang, Z.L., Li, H.M., Wu, H.Z., 2012. Matching relationship between faults and source rock and vertical migration characteristics of the oil in the Malang sag. *Acta Sedimentol. Sin.* 30, 1140–1148 (in Chinese with English abstract).
- MacGowan, D.B., Surdam, R.C., 1988. Disfunctional carboxylic acid anions in oilfield waters. *Org. Geochem.* 12, 245–259.
- Marinoni, N., Broekmans, M.A.T.M., 2013. Microstructure of selected aggregate quartz by XRD, and a critical review of the crystallinity index. *Cem. Concr. Res.* 54, 215–225.
- McHenry, I.J., 2009. Element mobility during zeolitic and argillic alteration of volcanic ash in a closed-basin lacustrine environment: case study Olduvai Gorge, Tanzania. *Chem. Geol.* 265, 540–552.
- Meshiri, I.D., 1986. On the reactivity of carbonic and organic acids and generation of secondary porosity. *Soc. Econ. Paleontol. Mineral.* 28, 123–128.
- Murata, K.J., Norman, M.B., 1976. An index of crystallinity for quartz. *Am. J. Sci.* 276, 1120–1130.
- Nagashima, K., Tada, R., Tana, A., 2007. Contribution of Aeolian dust in Japan Sea sediments estimated from ESR signal intensity and crystallinity of quartz. *Geochem. Geophys. Geosys.* 8, 1002–1004.
- Nelson, J., 1992. Are crustal thickness variations in old mountain belts like the Appalachians a consequence of lithospheric delamination. *Geology* 20, 498–502.
- Peng, H.J., Wang, X.W., Tang, J.X., Wang, D.H., 2010. The application of quartz cathodoluminescence in study of igneous rock. *Rock Miner. Anal.* 29, 153–160 (in Chinese with English abstract).
- Qiu, X.W., Liu, C.Y., Mao, G.Z., Deng, Y., Wang, F.F., Wang, J.Q., 2014. Late Triassic tuff intervals in the Ordos basin, Central China: their depositional, petrographic, geochemical characteristics and regional implications. *J. Asian Earth Sci.* 80, 148–160.
- Qiu, X.W., Liu, C.Y., Mao, G.Z., Wu, B.L., 2011. Petrological-Geochemical characteristics of volcanic ash sediments in Yanchang formation in Ordos Basin. *Earth Science-J. China Univ. Geosci.* 36, 139–150 (in Chinese with English abstract).
- Stein, R., 1986. Organic carbon and sedimentation rate—further evidence for anoxic deep-water conditions in the Cenomanian/Turonian Atlantic ocean. *Mar. Geol.* 72, 199–209.
- Stein, R., 1990. Organic carbon content/sedimentation rate relationship and its paleoenvironmental significance for marine sediments. *Geo-Mar. Lett.* 10, 37–44.
- Sun, F.H., Chen, X., Wang, Z.P., 2004. Diagenesis and division of diagenetic stage of deep strata series in Anpeng area, Biyang Sag. *J. Xi'an Shiyou Univ. Nat. Sci. Ed.*

- 19, 24–27 (in Chinese with English abstract).
- Tan, K.J., Zhang, F., Pan, J.G., Xu, D.N., Huang, L.J., Chen, Y.B., 2012. Quantitative prediction technology of high quality volcanic reservoir and its application. *Nat. Gas Sci.* 23, 175–180.
- Thomas Kalan, H.P., Sitorus, M.E., 1994. Jatibarang field, geologic study of volcanic reservoir for horizontal well proposal. In: Indonesian Petroleum Association, 23rd Annual Convention Proceedings, vol. 1, pp. 229–244.
- Thompson, M.D., Hermes, O.D., 1990. Ash-flow stratigraphy in the Mattapan volcanic complex, greater Boston, Massachusetts. *Geol. Soc. Am. Spec. Pap.* 245, 85–96.
- Tissot, B., Welte, D.H., 1984. Petroleum Formation and Occurrence. Springer Verlag, Berlin.
- Tomaru, H., Lu, Z.L., Fehn, U., Muramatsu, Y., 2009. Origin of hydrocarbons in the Green Tuff region of Japan: ^{129}I results from oil field brines and hot springs in the Akita and Niigata Basins. *Chem. Geol.* 264, 221–231.
- Wang, P., Pan, J.G., Wei, D.T., 2011. A new type of hydrocarbon source rock-sedimentary tuff. *J. Xi'an Shiyou Univ.* 26, 19–22 (in Chinese with English abstract).
- Wang, P.J., Wu, H.Y., Pang, Y.M., Men, G.T., Ren, Y.G., 2006. Volcanic facies of the Songliao Basin :Sequence, model and the quantitative relationship with porosity and permeability of the volcanic reservoir. *J. Jilin Univ. Earth Sci. Ed.* 36, 805–812.
- Wark, D.A., Hildreth, W., Spear, F.S., Cherniak, D.J., Watson, E.B., 2007. Pre-eruption recharge of the Bishop Magma system. *Geology* 35, 235–238.
- Winchester, J.A., Floyd, P.A., 1977. Geochemical discrimination of different magma series and their differentiation products using immobile elements. *Chem. Geol.* 20, 325–343.
- Wolff, D., Gislason, S.R., Oelkers, E.H., Putnis, C.V., 2004. The dissolution rates of natural glasses as a function of their composition at pH 4 and 10.6, and temperatures from 25 to 74 °C. *Geochim. Cosmochim. Acta* 68, 4843–4858.
- Xi, K.L., Cao, Y.C., Yang, C.Y., 2012. Diagenesis and diagenetic stage division of Es₄ reservoir in Langgu Sag. *Fault-Block Oil Gas Field* 19, 583–587 (in Chinese with English abstract).
- Xiao, W.J., Windley, B.F., Badarch, G., Sun, S., Li, J.L., Qin, K.Z., Wang, Z.H., 2004a. Palaeozoic accretionary and convergent tectonics of the southern Altaiids: implications for the lateral growth of Central Asia. *J. Geol. Soc.* 161, 339–342.
- Xiao, W.J., Zhang, L.C., Qin, K.Z., Sun, S., Li, J.L., 2004b. Paleozoic accretionary and collisional tectonics of the Eastern Tianshan (China): implications for the continental growth of central Asia. *Am. J. Sci.* 304, 370–395.
- Xu, H., Tang, D.Z., Zhang, J.F., 2013. Coexistence mechanism of multi-types of reservoir pressure in the Malang depression of the Santanghu Basin, China. *J. Pet. Sci. Eng.* 108, 279–287.
- Yang, X.Z., 1993. The devitrification of acid volcanic glass. *Resour. Surv. Environ.* 4, 73–81 (in Chinese with English abstract).
- Zhang, B.Q., Yu, H.Z., Jiang, Z.X., Wang, Y.J., Wang, W.H., 2003. Characteristics and diagenetic environments of source rocks by cathodoluminescence. *Pet. Explor. Dev.* 30, 117–120.
- Zhao, H.L., Huang, W., Wang, C., Di, Y.J., 2009. Micropores from devitrification in volcanic rocks and their contribution to reservoirs. *Oil Gas Geol.* 30, 47–52 (in Chinese with English abstract).
- Zhao, J.B., Chen, H.Y., Song, Y.G., Sun, Y.B., 2012. Determination of quartz content and crystallinity Index from loess samples. *Mar. Geol. Quat. Geol.* 32, 131–135 (in Chinese with English abstract).
- Zhao, X.Z., Li, Q., Jiang, Z.X., Zhang, R.F., Li, H.P., 2013. Organic geochemistry and reservoir characterization of the organic matter-rich calcilutite in the Shulu Sag, Bohai Bay Basin, North China. *Mar. Pet. Geol.* 51, 239–255.
- Zhu, Y.F., Zhang, L.F., Gu, L.B., Guo, X., 2005. The zircon shrimp chronology and trace element geochemistry of the Carboniferous volcanic rocks in western Tianshan Mountains. *Chin. Sci. Bull.* 50, 2201–2212.
- Zou, C.N., Zhu, R.K., Wu, S.T., Yang, Z., Tao, S.Z., Yuan, X.J., 2012. Types, characteristics, genesis and prospects of conventional and unconventional hydrocarbon accumulations: taking tight oil and tight gas in China as an instance. *Acta Pet. Sin.* 33, 173–187.